

Segmentation of Electron Microscopic Images with Artificial Gravitational Field for Enhancement of Visibility

Jonathan Tri Pham¹

¹(Department of Natural Sciences/ Tulane University, USA)

Abstract:

Background: Images obtained from an electron microscope are generally difficult for human experts to analyze due to their monochromatic nature that limits the data range necessary for differentiate features. This difficulty can lead to overlooking important features surrounded by a background of similar pixel intensities. While there exist various software for image enhancement, these software applications often require tedious and time-consuming manual adjustments that are good for artistic purpose but not appropriate for massive operation in a biological laboratory setting. For this reason, it is proposed in this paper a new automated technique of image enhancement to improve the visibility of the features in a monochromatic images from an electron microscope so that they can be easily analyzed by human experts.

Materials and Methods: In the development of the new automated image enhancement technique, the histogram of each monochromatic image is prepared, and this histogram is analyzed with a new segmentation algorithm that automatically and efficiently separates the histogram data into various clusters according to the values and proximity of the data. This new segmentation does not require any prior knowledge such as the number of clusters or the distribution of the data associated with existing segmentation algorithms, thus eliminating the requirement that an analyst of biological specimen must understand data clustering techniques in order to segment an image. Each cluster will be colorized in an expanding color range to permit better visualization of the features represented by the cluster. The colorization scheme is also automated according to the color perception of human eyes, thus enhancing the visibility of the features represented by the clusters while providing a seamless preprocessing operation that requires absolutely no intervention from human.

Results: The monochromatic images obtained from an electron microscope in a cell study are processed and colorized into enhanced images with much better visibility of features that permits an effective analysis by human experts. The same processing method is also applied to other types of monochromatic images such as x-ray images, infrared images, etc. to show a wide range of applicability of the method.

Conclusion: Automated preprocessing of monochromatic images from an electron microscope is an important task of preparing a massive amount of images for human to effectively analyze them in a laboratory setting. The combination of automated segmentation and automated colorization of monochromatic images presented in this paper delivers an efficient and effective

Key Word: Artificial gravitational field; Image segmentation; Clustering; False color representation

Date of Submission: 26-09-2020

Date of Acceptance: 09-10-2020

I. Introduction

Electron microscopy^{1,2,3,4} is the use of a special microscope that provides extremely high power magnification to study specimen in fine details. Due to the sophisticated use of electron beams to scan a specimen^{5,6,7,8}, high power magnification was achieved and fine details of a scanned specimen can be revealed. However, also due to this use of electron beams, the final results will be recorded as a spatial two-dimensional representation of the strength of the beams. Thus, it is common to see that the results of electron microscope scanning being shown as monochromatic images, e.g., in black and white images with many grey levels.

Since electron microscopy can provide images with much higher magnification than optical microscopy, the use of electron microscopy is becoming common in studies of biological specimens^{9,10,11,12,13}. However, when electron microscope was introduced, biological specimens were already observed through traditional optical microscopes that provide moderate magnification. In this setting, it was common practice to use dye to color specimens in a process called staining^{14,15,16,17} so that contrasting details can easily be seen with human eyes. However, the use of electron microscope, while providing high magnification, will only render monochromatic images. Therefore, when specimens appear transparent to the electron beam, it is common practice to stain them with heavy metals to enhance the contrasts between their internal structures. In this aspect, it is implied that the electron microscope images are viewed in their monochromatic form with the general belief that artificial coloring will not yield any new information.

While it is technically correct that artificial coloring of monochromatic images will not yield any new information, the existing information in monochromatic images can easily be obscured and be overlooked by human eyes due to many factors. In many scenarios of studying cells using electron microscopy, the resulting monochromatic images might contain the crucial information but this information might not be apparent to the human eyes of a viewer due to the limitation of digital coding scheme^{18,19,20,21}, display devices^{22,23}, and human visual acuity^{24,25,26,27}. Furthermore, it is also common to be mentally fatigued and overlook something when a person must analyze many monochromatic images of similar nature in a repetitive manner^{28,29,30,31} in a professional laboratory setting. Additionally, repetitive work in the laboratory can cause mental complacency that reduces the mental alertness to detect unexpected anomaly^{32,33,34,35}.

To combat mental fatigue and mental complacency when working with monochromatic data, it is a well-known common practice to highlight important data with colors so that it (the important data) will stand out to capture the attention of the viewer^{36,37,38,39}. This technique is useful when the data (e.g., text) is presented on paper and with the use of a color highlighting pen, important data can be marked to alert the reader that certain section of data on the paper is important. In this aspect, the no new data was created, the original data remains the same, but the viewer can easily focus the attention to important section of the data. The technique of highlighting important data has been used effectively by students studying textual contents in a traditional textbook^{40,41,42,43}, where texts are printed in black ink on the white paper of a text book. This practice is effective to the point that the publishers nowadays routinely print their textbooks with colors highlight of important sections as an aid to effective study.

This paper proposes the use of contrasting color to highlight different segments of monochromatic images from electron microscopes in the manner that will enhance the appearance of the features of the images to improve human visual acuity, thus addressing the problem of human overlooking obscured information in a monochromatic image described in previous paragraphs. In this aspect, a monochromatic image is partitioned into many segments, with each segment containing a group of pixels with similar values representing a feature. Each segment is colored with various shades of a selected color in the manner that the original image is transformed into a vibrant color image with image features readily stand out to capture the attention of human performing visual analysis. First, the process is performed manually to demonstrate feasibility. Then the process is automated to allow massive processing of many images in a professional laboratory. An example is given for the analysis of electron microscopic images during a routine calibration where it was noticed that many tiny granules appeared around the nucleus of a cell.

The automating of the process of false color representation of a monochromatic image consists of three steps: (i) segmentation of an image, (ii) colorization of each segment, and (iii) selection of colors to enhance features. In this paper, the segmentation of an image is based on the 1-dimensional histogram analysis, where features can be identified as a group of pixels accumulating at a specific value. Traditional segmentation process in data mining, while easy and simple to implement, normally requires a lot of computational resources and does not guarantee the results within some reasonable timeframe due to the iterative nature of the process. In order to bypass this tedious computational process, a newly developed technique of creating artificial gravitational field^{44,45} associating with data in the histogram is used, and the value and direction of the artificial gravitational field can give direct indication of which segment the data belongs to. This technique yields direct results immediately in one iteration (as opposed to an undetermined number of iterations in traditional segmentation process). The colorization of each segment is shown to be a simple linear transformation of grey data into color data. The selection of colors for each segment is developed around the color theory where colors are arranged in the color wheel in the order of increasing contrast. By modelling the contrasting order with the RGB (red, green, blue) representation of a color, an automatic sequence of contrasting colors can be generated to be used in the colorization of the segments.

Numerical results are given in analyzing electron microscopic images to identify unexpected tiny granular objects that appeared just around the nucleus of a cell during the routine calibration of a new electron microscope to demonstrate workability of the false color representation. Future works are given in analyzing thermal images, x-ray images, and ultrasound images to demonstrate extensibility of the false color representation to a wide range of applications. Thermal images collected from field study of wheat plants are colorized to allow analysts better view of the plant features. Furthermore, thermal images are used in the experimental study of identifying human body in a search and rescue mission. X-ray images and ultrasound images are colorized to allow medical technicians a better view of the internal structure of the human body.

II. Background: Histogram Analysis of Electron Microscope Images

A histogram of an image^{44,45,46} (i.e., Hu, et. al., 2014; Han, et. al., 2011; Kim, et. al., 2001;) is a listing of frequencies of occurrence of each possible pixel value in that image. Thus, when the value of a pixel of a monochromatic image from an electron microscope is just a scalar quantity, the histogram of the image is a one-

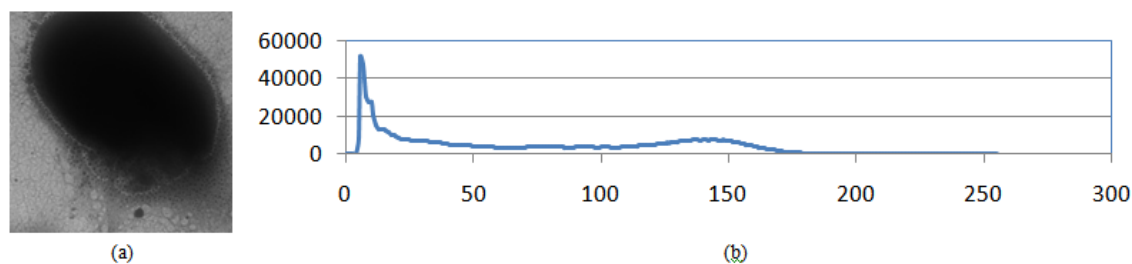


Figure 1. (a) a monochromatic image of a cell nucleus, and (b) its corresponding histogram showing a concentrated group of pixels in the range of 1 – 50, and another concentrated group of pixels in the range 100 – 170.

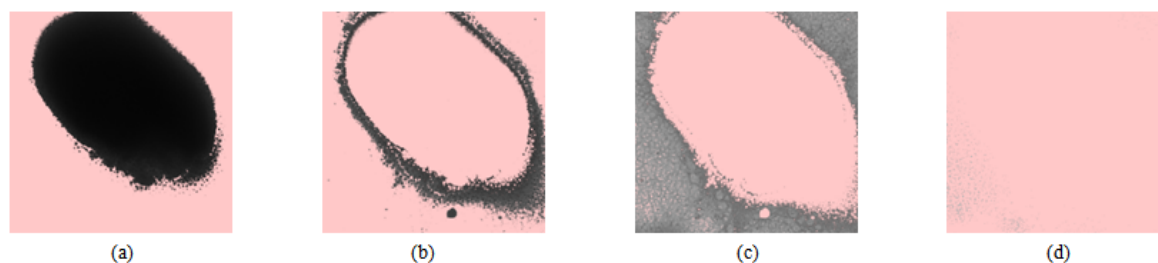


Figure 2. Separation of an image according to histogram analysis: (a) pixels in the range of 0 – 50, (b) pixels in the range of 51 – 99, (c) pixels in the range of 100 – 170, and (d) pixels in the range of 171 – 255.

one relation between an independent variable (pixel value) and a dependent variable (frequency of occurrence), and can be plotted in a 2-dimensional graphic. Figure 1 shows a monochromatic representation of an electron scan (of a cell), and its corresponding histogram. In this example, the strength of an electron beam is encoded into a range of 0 to 255 associated with the 8-bit representation of a black and white digital image. In this display, the pixel value 0 is shown as the darkest (black color), the pixel value 255 is shown as the lightest (white color), and the pixel value between 0 and 255 is shown as various grey levels corresponding to the gradual changes of color between the two extreme values 0 (darkest) and 255 (lightest).

In a digital monochromatic image, from one pixel to another adjacent pixel, the values between them either do not vary very much to form a spatial smooth transitioning typically seen in a feature, or vary a lot to form a sharp contrasting typically seen at the boundary between features. In this aspect, pixel values are useful in analyzing and processing a digital image. In looking at the histogram of a monochromatic image, it can be easily seen that pixels are concentrated at certain band region, and this concentrated group of pixels normally represents a specific feature in the image. The concentration at a band region, where a band is specified by a minimum pixel value and a maximum pixel value, occurs in the form of a bell curve, with the maximum at the center, and the gradual decrease on both sides of the maximum. Figure 1(b) shows a histogram of the image in Figure 1(a), and this histogram shows two band regions with high concentration of pixels: the first band region between 0 and 50 where the maximum occurrence is at around the value 10, and the second band region between 100 and 170 where the maximum occurrence is at around the value 140. In between these two band regions, there is a flat region in the band between 51 and 99, and another flat region in the band between 171 and 255.

Figure 2 shows the separation of the image in Figure 1(a) into four segments according to pixel values. The first segment in Figure 2(a) consists of pixels with values between 0 and 50. This is the region with the darkest color in the image. By visual inspection, the dark oval shape in 2(a) corresponds to the nucleus of the cell. The third segment in Figure 2(c) consists of pixels with values between 100 and 170. This is the region with fairly light color in the image. Again, by visual inspection, the light color texture in 2(c) corresponds to the cytoplasm of the cell. The second segment in Figure 2(b) consists of pixels with values between 51 and 99, the flat band region between the two features in the band region between 0 and 50 and the band region between 100 and 170. However, by visual inspection, this flat band region between 51 and 99 actually corresponds to the tiny granular objects surrounding the nucleus of the cell. Similarly, the flat band region between 171 and 255 that is beyond the feature in the band region between 100 and 170 corresponds to a group of tiny freckles in one local area within the cytoplasm of the cell.

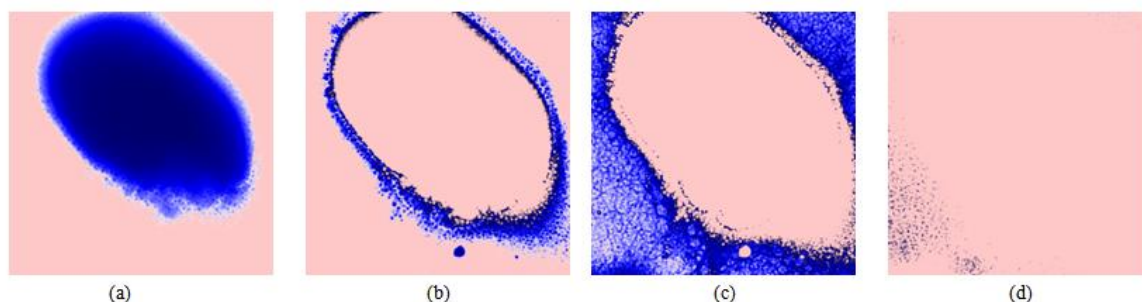


Figure 3. Assigning false colour (blue) representation for images from Figure 2 can enhance the visibility of details in each range: (a) pixels in the range of 0 – 50, (b) pixels in the range of 51 – 99, (c) pixels in the range of 100 – 170, and (d) pixels in the range of 171 – 255.

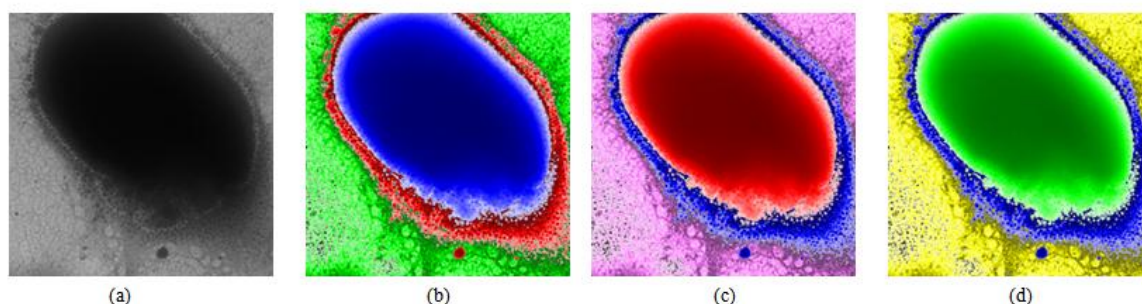


Figure 4. Assigning contrasting false colour representation enhance the visibility of details in overall picture: (a) original image, (b) colour scheme blue-red-green-black for the 4 bands shown in Figure 3, (c) colour scheme red-blue-magenta-black for the 4 bands shown in Figure 3, and (d) colour scheme green-blue-yellow-black for the 4 bands shown in Figure 3.

By analyzing the histogram of a monochromatic image, one can identify various band regions where pixels are heavily concentrated to the form of a bell curve in each region. By isolating pixels that have values within each band region, one can extract a segment of the image corresponding to a specific feature of that image. This process of identifying four band regions in the example of Figures 1 and 2 from analyzing the histogram of an image is fairly simple with the intelligent mind of a human, but can be difficult to code into a computer program due to fluctuation of data in the histogram. Furthermore, the number of band regions is not known in advance, making it even more difficult to formalize the process into programming codes instructing the computer of what to do specifically.

III. False Color Representation

False color representation is the assignment of colors to certain section of a monochromatic image to enhance the visual effect. Thus, the key element to assigning false color representation to a monochromatic image is the identification of a section of the image where a color is assigned and applied. In this aspect, a section of an image that is identified for colorization is normally associated with a feature of that image. Therefore, false color representation of a monochromatic image consists of three steps: (i) identification of sections in an image for colorization, (ii) selection of colors to assign to the identified sections, and (iii) application of a color to each section to transform the monochromatic image into a color image.

A monochromatic image, such as one shown in Figure 1(a) can be separated into different segments according to the range of pixel values, where each range is determined through some types of analysis. Figure 1(b) shows the histogram of the image, with a quick visual analysis indicating that pixels with values from 0 to 50 seem to form a segment, and pixels with values from 100 to 170 seem to form another segment. The remaining two ranges, from 51 to 99 and from 171 to 255 show flat distribution and therefore might be just transitioning filler. Figure 2 shows the separation of Figure 1(a) into four segments according to this analysis of the histogram, and the first segment consisting of pixels with values between 0 and 50 represents the nucleus of the cell, the second segment consisting of pixels with values between 51 and 99 represents the surrounding of the nucleus of the cell, the third segment consisting of pixels with values between 100 and 170 represents the cytoplasm of the cell, and the fourth segment consisting of pixels with values between 171 and 255 represents unidentified speckles in the cytoplasm of the cell.

For each segment shown in Figure 2, a color can be used to colorize it. In Figure 3, the color blue is arbitrarily used to colorize each segment. In this aspect the color blue is used in 256 various shades, ranging from the lightest shade (white) to the darkest shade (blue). In this assignment, pixel values from 0 to 50 are linearly transformed so that the value 0 will correspond to the darkest shade (blue) and the value 50 to the

lightest shade (white). This linear transformation represents a stretching in color range, allowing more differentiation between pixel values. Thus, while Figure 2(a) seems to show a monotonic black object, but under the stretching effect of the linear transformation Figure 3(a) seems to show more details to human eyes. Similarly, the other segments in Figure 2 are colorized with the arbitrarily selected color blue. Again, the stretching effect shown in Figure 3 seems to allow more details to appear to human eyes.

If each of the four segments (shown in Figure 2) of the original image (shown in Figure 1(a)) is colorized with a different color in the way that one segment will contrast to another segment, the image can easily appear vibrantly different to the human eyes in the manner that the whole image is easy to analyze with respect to individual features of the image. Figure 4 shows the original monochromatic image, and three different schemes of colorization where different combinations of colors are selected and assigned to each of the four segments identified in Figure 2. While the combinations of colors are arbitrarily selected for Figure 4, the resulting images show marked difference from the original image in terms of the enhanced visibility of the features that in theory should allow better visual analysis, especially in the laboratory condition where many images must be analyzed efficiently and effectively. Thus, it is important to select colors for the segments in the manner that the features in an image must stand out in an obvious manner to the human eyes of the people responsible for the analysis of the images.

The three steps in the process of false color representation of a monochromatic image, (i) identification of sections in an image for colorization, (ii) selection of colors to assign to the identified sections, and (iii) application of a color to each section to transform the monochromatic image into a color image, can be done manually as described in the example shown in Figures 1 through 4. However, this process will become repetitively tedious when many images must be colorized for the analysis. Thus, the fatigue factor associating with human having to analyzed many monochromatic images that can affect the result of the analysis, while seemingly resolved through colorization, has a new cost at causing fatigue associating with human having to manually colorize many monochromatic images that can affect the resulting colorization, and in turn affecting the analysis. For this reason, if the colorization can be done automatically, the original problem is resolved without the new cost just mentioned about the fatigue caused by the repetitively tedious task of colorization. The two challenging things in automating the process of colorization are the segmentation of an image into many segments, and the selection of contrasting colors to assign to each segment of an image.

IV. Analysis of colors in assigning false color representation

Colors have been used for years by artists in painting their pictures to depict the scenery that they see. In this line of work, it was noted, through the perception of human eyes, that a color normally will appear more vibrant when placed next to a certain other color. Thus, to emphasize on an object, artists often choose the background color in the manner that the object will appear more vibrant to the eyes of the viewers. The two colors selected to give this vibrant effect are said to be contrasting. This practice eventually became part of the theory of colors^{47,48,49} (Chevreul, 2015; Albers, 2013; von Goethe, 2006) that formally defines colors and their relation in terms of how they are formed from basic color elements, and how they are arranged in smooth transitioning order as well as in contrasting pairs.

In modern days when imaging is computerized, colors have been coded into numerical representation mainly for the purpose of instructing the displaying unit such as printers and monitors how to show the color (represented by the code) for visualization. In this aspect, there are various coding schemes used by software for working with colors. These schemes, even though being different in organization structure, use the same original color theory that a few basic color elements can be combined in various levels to create a full spectrum of colors visible to the human eyes. In this aspect, the color model RGB using the three basic colors red, green, and blue (thus the acronym RGB in the name) is commonly used in coding for displaying purpose; while the color model CMYK using the four basic colors cyan, magenta, yellow, and black (thus the acronym CMYK in the name) is commonly used in coding for printing purpose. While both coding schemes are equivalent (there exist mathematical transformations that convert the code in one scheme to code in another scheme), each scheme is developed for satisfying the physical capability of the type of the devices (monitors or printers). However, the RGB color scheme is also commonly used for file storage of an image. Thus, most processing procedures were developed around the RGB color scheme because of the data is readily available from the direct reading of the image file.

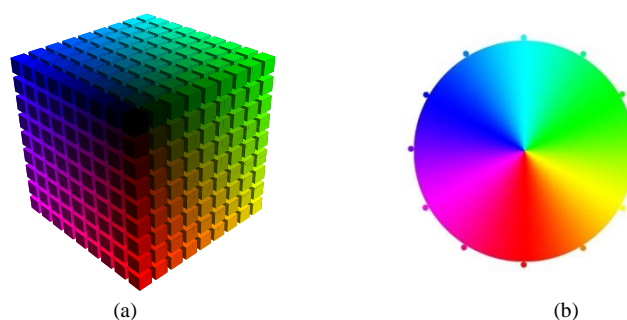


Figure 5. In the RGB colour model, the three basic colours Red, Green, and Blue are used in various combinations to create a full visible spectrum of colours: (a) full spectrum in a 3-D colour space, (b) 2-D colour wheel.

Figure 5(a) shows the colors spectrum generated by the RGB color model. Extracted from this spectrum is a subset of colors generated from combining two of the three primary colors in various portion to form a continuous spectrum of secondary colors shown in Figure 5(b). In this Figure, the colors are arranged into a color wheel according to the color theory where the two contrasting colors are placed opposite to each other from the centre of the wheel. The three primary colors red, green, and blue are placed equidistant from each other in the polar coordination, and the transitioning colors in between them are generated by combining various degrees of colors between the two adjacent primary colors, creating a smooth transitioning. In this wheel, the three secondary colors yellow, cyan, and magenta are generated by combining equal portion of red and green to create yellow, equal portion of green and blue to create cyan, and equal portion of red and blue to create magenta. Similarly, the six tertiary colors raspberry, violet, ocean, turquoise, spring green, and orange are created by combining equal portion of two adjacent colors (from the set of three primary and three secondary colors) on the wheel. This procedure of combining adjacent colors continues indefinitely to create a continuous color wheel in Figure 5(b).

Observing the color wheel in Figure 5(b), it is noted that any pair of colors on the opposite sides of each other across from the center of the wheel are considered completely contrasting (at the maximum contrasting level). As the colors move closer to each other, the contrasting level reduces. In this aspect, the 12 colors in Figure 5(b) can be grouped into six pairs of completely contrasting colors: red-cyan, raspberry-turquoise, magenta-green, violet-spring green, blue-yellow, and ocean-orange. Considering the pair of contrasting colors red-cyan, since the two colors ocean and turquoise are close to the color cyan on the color wheel, they can form two pairs of nearly contrasting colors with red: red-ocean, and red-turquoise. To a computer analyzing the numerical values assigned to each color, there is a distinct difference between a pair of completing contrasting colors and a pair of nearly contrasting colors. However, to human eyes, there is only a slight difference between the two pairs that is hardly noticeable, therefore giving people working with colors a wide range of color selection for creating visual effects with contrasting colors.

V. Automating the Process of False Color Representation

The process of false color representation of monochromatic images consists of three basic steps: (i) identification of segments in an image for colorization, (ii) selection of colors to assign to the identified segments, and (iii) application of a color to each segments to transform the monochromatic image into a color image. As described in previous sections, these steps can be done manually for a few images, but will become repetitively tedious when done manually for a large number of images. Thus, the need to automating this process of false color representation of monochromatic images is specifically important for laboratory environment where many images are routinely collected on a daily basis for various studies.

Segmentation of an image

Segmentation is the task of separating a large set of data points into smaller subsets. Even though these resulting smaller subsets are presumably non-overlapping in the original context of segmentation, there are special cases where the subsets are allowed to be overlapping, for example when fuzzy sets are used there will be overlapping regions between the subsets. In the context of this study, it is assumed that non-overlapping is the characteristic of the resulting subsets of data points. In general, each subset of data contains a numbers of data points that share similar characteristics, and thus will appear closer to each other when shown in a data space where each dimension of the data space represents one characteristic describing the data. Figure 6(a) shows examples of a set of data that can be separated into two subsets, shown in Figure 6(b), of common

characteristics (proximity) in a 2-dimensional space (even though the focus on the histogram of monochromatic images being one dimensional, the example here is better for visualization).

The concept of creating an artificial gravitational field for the purpose of segmentation treats each data point as a point mass with artificial mass m that can generate an artificial gravitational field around it with the pulling effect on other data points situated in the same data space. Thus, when data points are concentrated in a particular location, they create a strong gravitational field pulling them toward their centre of mass. Using Newtonian law of gravity, the artificial gravitational field created by each data point situated at coordinate r_k is given as

$$F(r) = G \frac{m}{\|r_k - r\|^2} \cdot \frac{(r_k - r)}{\|r_k - r\|}, \quad (1)$$

where r is the location where the field by the mass m located at r_k is exerting effect, and G is the gravitational constant. Since data mass, distance, and the gravitational field are artificially created and therefore do not have to follow the exact calculated effect of real mass and real distance in the universe, both the mass m and the gravitational constant G can be set to the value 1 and the distance unit can also be arbitrarily used to simplify the computation without loss of generality. Figure 6(c) shows the direction of the artificial gravitational field where a point mass if placed in the 2-dimensional space will experience the pulling effect of the field. Outside each cluster, the gravitational field uniformly converges to the two centres of mass of the two clusters. However, inside each cluster, the gravitational field can fluctuate due to the use of the value 1 for the gravitational constant G and the unit mass m with respect to the spatial unit of the location. By analysing the direction of the artificial gravitational field, it is possible to determine the clusters of point masses that are pulled to the common centre of mass.

For a 1-dimensional data space of a histogram of a monochromatic image, the pixels are distributed between the values of 0 and 255. The histogram is showing how many pixels in the image are the same at a particular given value. Assigning an artificial mass $m = 1$ to each pixel, the artificial gravitational field can be calculated in this 1-dimensional space using equation (1). Figure 7 uses the same monochromatic image of Figure 1(a) and its corresponding histogram of Figure 1(b). The corresponding artificial gravitational field shown in 7(a) is given in terms of both magnitude (representing the strength of the field) and direction (positive value, indicated by the black arrows, means rightward and negative value, indicated by the red arrows, means leftward). Notice that due to the scaling factor, the field value can appear near the horizontal axis and is difficult for manual analysis, therefore a plot in pink colour showing either the value of 20,000 for positive field value, and $-20,000$ for negative value to allow easy manual analysis at this stage. In this aspect, a cluster of point masses will create an artificial gravitational field that points toward it, i.e., from the left of the cluster the field is pointing rightward to the cluster, and from the right of the cluster the field is pointing leftward to the cluster. By this simple rule, the artificial gravitational field in Figure 7(a), shown in purple colour, can be used to separate the pixels into various clusters. Every cluster should consists of contiguous point masses starting from the left with artificial gravitational field pointing rightward (the value being positive) until it reaches a point where the artificial gravitational field shifts direction to pointing leftward (the value being negative), and ends at the point where the artificial gravitational field shift direction again to pointing rightward (the value being positive). At this shift of direction from pointing leftward to pointing rightward, a new cluster is identified. Thus Figure 7(a) shows a total of 6 clusters, with cluster 1 consisting of pixels with values from 0 to 67, cluster 2 consisting of pixels with values from 68 to 87, cluster 3 consisting of pixels with values from 88 to 98, cluster 4 consisting of pixels with values from 99 to 104, cluster 5 consisting of pixels with values from 105 to 138, and cluster 6 consisting of pixels with values from 139 to 255. Figure 7(b) shows the histogram of Figure 1(b) again, this time in 6 different colours indicating 6 different segments. Figure 8 shows the actual six segments corresponding to the clusters on the histogram, with each segment being coloured with an arbitrary colour, and afterward these coloured segments are recombined into the final false colour representation. The automated process of selecting colours will be presented in the next subsection, and the assignment of each colour to a pixel range will be presented in the subsection after the next subsection.

The algorithm of separating an image $I(n, m)$ of size $N \times M$, i.e., $0 \leq n < N$ and $0 \leq m < M$, into different segments can be summarized as follows:

- (1) Prepare a histogram array $h(p)$ for $p = 0, 1, \dots, 255$ as follows

$$h(p) = \sum_{n=0}^{N-1} \sum_{m=0}^{M-1} \eta_p(I(n, m)), \quad (2)$$

where

$$\eta_p(I(n, m)) = \begin{cases} 1, & \text{if } I(n, m) = p, \\ 0, & \text{else.} \end{cases} \quad (3)$$

- (2) Prepare an artificial gravitational field array $F(p)$ for $p = 0, 1, \dots, 255$ as follows

$$F(p) = \sum_{\substack{q=0 \\ q \neq p}}^{255} \frac{h(q)}{(q-p)^2} \cdot \frac{(q-p)}{|q-p|}. \quad (4)$$

(3) Initialize S , the number of segments, to be 1. Initialize the minimum value for cluster number S to be $\theta_{\min}(S) = 0$.

(4) Start from index $p = 1$, given that Equation (4) always yields $F(0) > 0$ because all the mass points are to the right of this location and will exert a positive pull, and $F(255) < 0$ because all the mass points are to the left of this location and will exert a negative pull, examine the values $F(p-1)$ and $F(p)$ according to the following rule.

Rule: If $F(p-1) < 0$ and $F(p) \geq 0$ then:

- (i) increase S by 1, i.e., $S = S + 1$,
- (ii) set the maximum value of cluster $S - 1$ to be

$$\theta_{\max}(S-1) = p-1,$$

- (iii) set the minimum value of cluster S to be

$$\theta_{\min}(S) = p. \quad (5)$$

(5) Increase p by 1, i.e., $p = p + 1$, and repeat the Rule in Step (4) until after $p = 255$.

(6) After exiting the repetition structure in (4) and (5), set the maximum value for cluster number S to be $\theta_{\max}(S) = 255$. The total number of clusters is S .

(7) Start from index $s = 1$, the subset $I_s(n, m)$ of the original image $I(n, m)$ that only contains pixels with values between $\theta_{\min}(s)$ and $\theta_{\max}(s)$ is

$$I_s(n, m) = \begin{cases} I(n, m), & \text{if } \theta_{\min}(s) \leq I(n, m) \leq \theta_{\max}(s), \\ \beta, & \text{else,} \end{cases} \quad (6)$$

(8) Increase s by 1, i.e., $s = s + 1$, and repeat Step (7) until after $s = S$.

The algorithm from (1) through (8) is non-iterative and therefore guarantees the completion within a fixed timeframe. The segmentation process basically merge a group of consecutive positive data points (of artificial gravitational field) together with the immediate next group of consecutive negative data points (of artificial gravitational field) to form a cluster, and the resulting segments are unique. Together the three Figures 1(b), 7, and 8 show an example that went through the automated process that is describe in the 8 steps above. The intermediate results are shown at each of the step.

Selection of contrasting/transitioning colors

A set of colours must be selected to colourise the segments extracted from an image. In some application, the users might prefer a smooth transitioning of the pixel values as it increases from the minimum to the maximum allowed value so that the image is more realistic. In some other application, the users might prefer a sharp change of one colour to another contrasting colour so that specific features in an image can be easily identified. For both preferences, it is possible to develop an increasing index system associating with the colour arrangement either for smooth transitioning or for sharp contrasting at the choice of the user.

As seen in the segmentation process discussed previously, a typical result normally consists of between 3 to 8 segments. Thus, the set of 12 colors (three primary colors red, green, and blue; three secondary colors cyan, yellow, and magenta; and six tertiary colors) identified in Figure 5(b) of Section 4 will be sufficient. Specifically, if a user decides on the mode of the color sequence (smooth transitioning or sharp contrasting), and selects one color as a starting point in the sequence, how would one program the computer in an order of increasing index from 0 (for the selected color as the starting point) toward the other 11 colors in the manner that corresponds to the mode of the color sequence. In order to address this coding problem, the colors are treated as numerical codes, and the sequence of color is modelled as a function dependent on the index that ranges from 0 to 11 (for 12 basic colors).

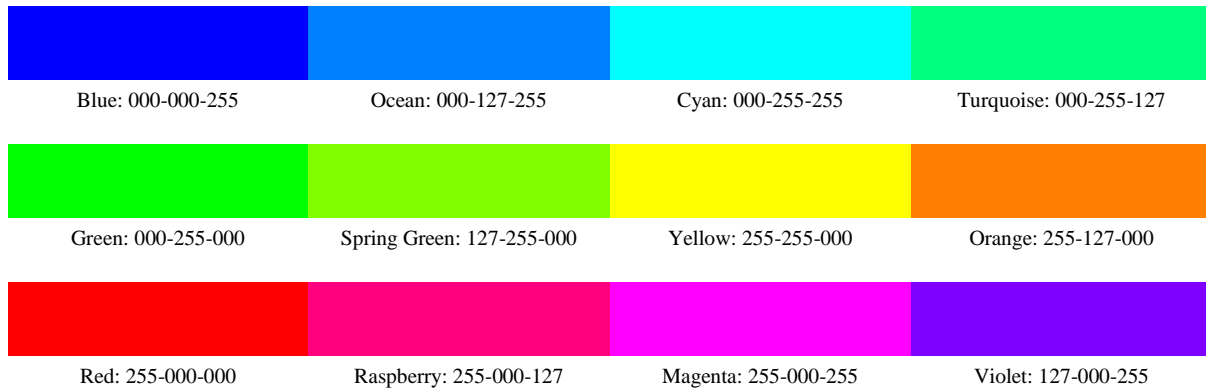


Figure 9. Twelve basic colours and their corresponding RGB codes.

From the color wheel in Figure 5(b), the twelve basic colors are shown in Figure 9. According to the color wheel, the smooth transition of colors dictates that they appear in the following sequence: blue, ocean, cyan, turquoise, green, spring green, yellow, orange, red, raspberry, magenta, and violet. Assigning the index 0 to blue, 1 to ocean, 2 to cyan, and so forth, the color modelling problem can be formulated as follows

$$\rho_{\text{smooth,blue}}(i) = [c_{\text{red}}(i) \quad c_{\text{blue}}(i) \quad c_{\text{green}}(i)]^T, \quad (7)$$

If this specific sequence of colors (blue, ocean, cyan, turquoise, green, spring green, yellow, orange, red, raspberry, magenta, and violet) can be mathematically modeled, where (6) can be formulated, any sequence with a selected color can be formed with the relation $\rho_{\text{smooth,colourX}}(i) = \rho_{\text{smooth,blue}}(i+n)$ where n is the index of the given color named colourX in the sequence of colors (blue (index = 0), ocean (1), cyan (2), turquoise (3), green (4), spring green (5), yellow (6), orange (7), red (8), raspberry (9), magenta (10), and violet (11)). Using the RGB values from Figure 5 for the twelve colors in the sequence, equation (6) is extended into Table 1. Examining this table reveals that the functions $c_{\text{red}}(i)$, $c_{\text{blue}}(i)$, and $c_{\text{green}}(i)$ are related as follows

$$c_{\text{blue}}(i) = c_{\text{red}}(i + 4), \quad (8a)$$

$$c_{\text{green}}(i) = c_{\text{red}}(i + 8). \quad (8b)$$

Further examining Table 1 for the function $c_{\text{red}}(i)$, the data shows a number series satisfying the formula

$$c_{\text{red}}(i) = \phi\left(\frac{i_{\text{mod}(12)}}{6}\right) \cdot 255 \cdot \left(1 - \phi\left(\frac{i_{\text{mod}(6)}}{5}\right)\right) + \phi\left(\frac{i_{\text{mod}(6)}}{5}\right) \cdot 127, \quad (8c)$$

where the function $\phi(\cdot)$ is the floor function returning the maximum integer that is smaller than the input argument, and the function $\text{mod}(n)$ is the modulo function returning the remainder of the division between the integer i and the base n .

For forming a contrasting sequence, instead of using maximum contrast (that will not permit a sequence), the near contrast scheme is used. Table 2 shows a sequence of near contrasting colors and their corresponding RGB values. Let $\rho_{\text{contrasting,blue}}(i)$ be a sequence of contrasting color starting with the color blue for the index $i = 0$, it can be seen that

$$\rho_{\text{contrasting,blue}}(i) = \rho_{\text{smooth,blue}}(5i_{\text{mod}(12)}), \quad (9)$$

Application of Colours to Segments of an Image

When a selected segment $S(s)$ is colorized with a specific color, the range $[p_{\text{min}}(s), p_{\text{max}}(s)]$ of pixel values of that segment is already known from the process of segmentation described previously. In an 8-bit coding scheme, the total range for all pixels is $[0, 255]$, therefore $0 \leq p_{\text{min}}(s) < p_{\text{max}}(s) \leq 255$, or the range $[p_{\text{min}}(s), p_{\text{max}}(s)]$ always has a smaller than or equal width of the total range $[0, 255]$. Thus, given a pixel value $p \in [p_{\text{min}}(s), p_{\text{max}}(s)]$, and given a selected color $\rho_{\text{smooth,blue}}(i)$ in the smooth transitioning sequence (or $\rho_{\text{contrasting,blue}}(i)$ in the contrasting sequence), the value p must be mathematically translated into a shade of the color $\rho_{\text{smooth,blue}}(i)$ or $\rho_{\text{contrasting,blue}}(i)$ in the manner that it can be coded in a computer program. For a smooth transitioning sequence, the range $[p_{\text{min}}(s), p_{\text{max}}(s)]$ must be translated to the range $[\rho_{\text{smooth,blue}}(i), \rho_{\text{smooth,blue}}(i+1)]$. The following simple scaling formula is proposed for this purpose

$$\Phi_{\text{smooth}}(p, \rho_{\text{smooth,blue}}(i)) = \rho_{\text{smooth,blue}}(i) +$$

Table 1. RGB component values for the twelve colors selected as a smooth transitioning sequence starting with the color blue.

colour	blue	ocean	cyan	turquoise	green	spring green	yellow	orange	red	raspberry	magenta	violet
i	0	1	2	3	4	5	6	7	8	9	10	11
$c_{red}(i)$	000	000	000	000	000	127	255	255	255	255	255	127
$c_{blue}(i)$	000	127	255	255	255	255	255	127	000	000	000	000
$c_{green}(i)$	255	255	255	127	000	000	000	000	000	127	255	255

Table 2. RGB component values for the twelve colors selected as a contrasting sequence starting with the color blue.

colour	blue	spring green	magenta	turquoise	red	ocean	yellow	violet	green	raspberry	cyan	orange
i	0	1	2	3	4	5	6	7	8	9	10	11
$c_{red}(i)$	000	127	255	000	255	000	255	127	000	255	000	255
$c_{blue}(i)$	000	255	000	255	000	127	255	000	255	000	255	127
$c_{green}(i)$	255	000	255	127	000	255	000	255	000	127	255	000

$$\frac{p - p_{\min}(s)}{p_{\max}(s) - p_{\min}(s)} \cdot (\rho_{\text{smooth,blue}}(i+1) - \rho_{\text{smooth,blue}}(i)). \quad (10)$$

Examining the RGB values of the colours in Tables 1 and 2, there will always a RGB component in two consecutive colours $\rho_{\text{smooth,blue}}(i)$ and $\rho_{\text{smooth,blue}}(i+1)$ that have the difference of 255, indicating a range with width 255. Thus, the linear translation of data in (10) for the smaller range $[p_{\min}(s), p_{\max}(s)]$ into a larger range $[\rho_{\text{smooth,blue}}(i), \rho_{\text{smooth,blue}}(i+1)]$ is effectively the magnification of the range, amplifying the separation between two consecutive values in the range $[p_{\min}(s), p_{\max}(s)]$ into a wider separation between two colours in the range $[\rho_{\text{smooth,blue}}(i), \rho_{\text{smooth,blue}}(i+1)]$. This effect should allow details hidden within a narrow range of gray colors to be seen in a wider range of selected color.

For a contrasting sequence, the range $[p_{\min}(s), p_{\max}(s)]$ must be translated into different shades of the selected colour $\rho_{\text{contrasting,blue}}(i)$. Using the convention that smaller value means darker shade and larger value means lighter shade, the scaling formula to translate data p in the range $[p_{\min}(s), p_{\max}(s)]$ into different shades of the colour $\rho_{\text{contrasting,blue}}(i)$ is proposed for this purpose. Recall that $\rho_{\text{contrasting,blue}}(i) = \rho_{\text{smooth,blue}}((5i)_{\text{mod}(12)})$, and using the relations in 8(a) and 8(b), the transformation therefore is formulated as,

$$\Phi_{\text{contrasting}}(p, \rho_{\text{contrasting,blue}}(i)) = \begin{bmatrix} \gamma(p, c_{red}(5i_{\text{mod}(12)})) \\ \gamma(p, c_{red}(5i_{\text{mod}(12)} + 4)) \\ \gamma(p, c_{red}(5i_{\text{mod}(12)} + 8)) \end{bmatrix}, \quad (11)$$

where

$$\gamma(p, v) = \begin{cases} 0, & \text{if } \tau(p) < 128 \text{ and } v = 0, \\ 127 - (3/4)(128 - \tau(p)), & \text{if } \tau(p) < 128 \text{ and } v = 127, \\ 255 - (3/2)(128 - \tau(p)), & \text{if } \tau(p) < 128 \text{ and } v = 255, \\ (3/2)(\tau(p) - 128), & \text{if } \tau(p) \geq 128 \text{ and } v = 0, \\ (3/4)(\tau(p) - 128), & \text{if } \tau(p) \geq 128 \text{ and } v = 127, \\ 255, & \text{if } \tau(p) \geq 128 \text{ and } v = 255, \end{cases} \quad (12a)$$

$$\tau(p) = \frac{p - p_{\min}(s)}{p_{\max}(s) - p_{\min}(s)} \cdot 256. \quad (12b)$$

Figure 10 shows different shades of each colour listed in Figure 9, generated with the given formulas in (11), (12a), and 12(b).

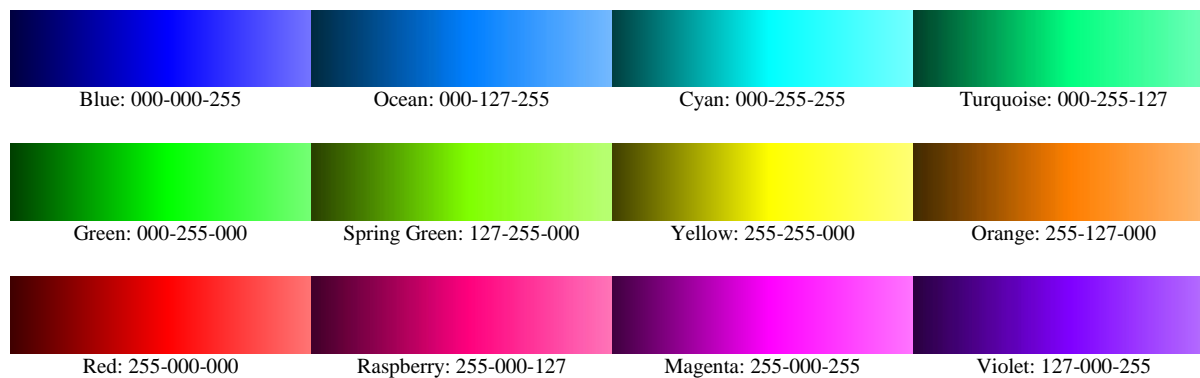


Figure 10. Twelve basic colours and their corresponding 256 shades (the RGB code is at the midpoint of the bar).

VI. Examples of cell study using electron microscope with false color representation

In a routine calibration of a newly acquired electron microscope, researchers were baffled at the appearance of small granular objects surrounding the nucleus of the cell prepared as a sample for the calibration, as shown in Figure 11(a). Unsure if these granular objects are parts of the cells, contamination during staining, or interference of additive noises during the transmission of data from microscope to computer, researchers prepared more samples and scanned them under various conditions in an attempt to eliminate the scenarios of contamination during preparation of samples, and electrostatic noise interference during the data transmission. Many images were collected, and reviewed manually by various personnel in the laboratory. In this review, it was subjectively concluded that “some” of the images showed, conclusively, the existence of tiny granular objects surrounding the cell nucleus, while “some” other images are inconclusive to the human eyes. While a hypothesis (that a cell nucleus, just before a cell dies, can release some biochemical by-product when it is stained with too much heavy metal) for the phenomenon was already formed as a basis for further investigation, it is important to objectively analyse the data through computer to confirm the phenomenon, especially with the inconclusive images where human eyes cannot detect what was observed in other conclusive images, before spending more resources pursuing the investigation based on the hypothesis. Thus, there is a need to isolate the image data of the area around the nucleus and enhance it for scrutiny in further inspection.

Traditional image editing software such as Photoshop does provide the capability of manually identifying a spatial region in an image for isolation and colour enhancement. However, the process is so tedious for the conclusive images, and very difficult for the inconclusive images where a spatial region of interest cannot be manually identified with human eyes. It is decided that computer software is needed to perform the task automatically to allow human analysts to view the enhanced images to conclusively confirm the phenomenon of the appearance of tiny granular objects around the nucleus of a cell. If the phenomenon is confirmed, then additional study can be conducted where cells are prepared in various amounts of stain, and scanned under the same environment condition for a statistical analysis of the correlation between the amount of stain and the amount of granular objects observed in the images. Figures 11 through 13 show some of the images processed for this initial analysis that required as a precursor to further studies. For all of the available images, the segments are efficiently identified and colourized in an automatic manner described in the previous sections, and all of these images are confirmed conclusively of the appearance of small granular objects around the nucleus. Furthermore, the granular objects seemed to scatter into the cytoplasm of the cell in the manner that supports the hypothesis that a cell nucleus, just before a cell dies, can release some biochemical by-product when it is stained with too much heavy metal.

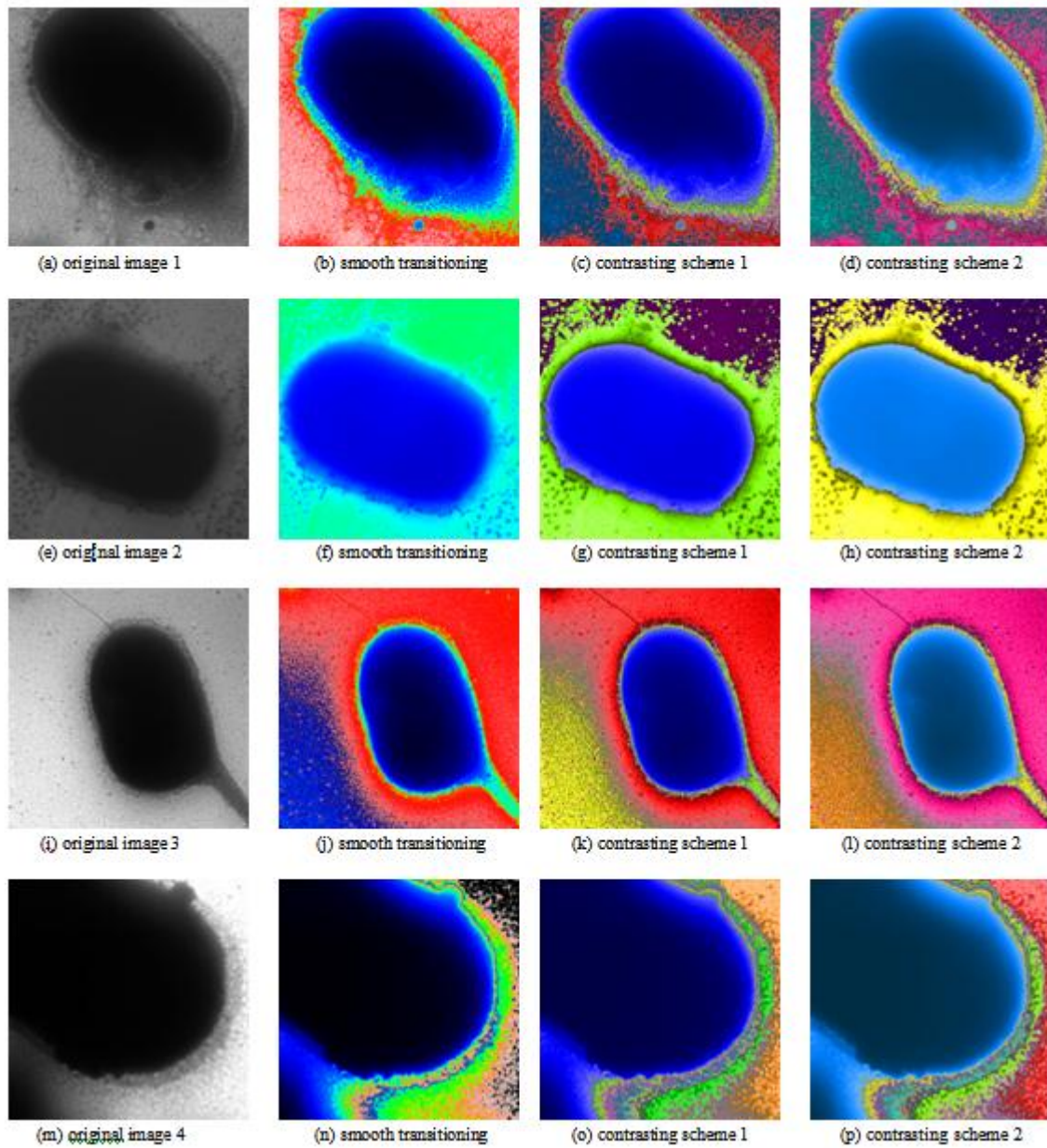


Figure 11. Segmentation of Set 1 of four electron microscope images of cells, with column 1 showing the original images, column 2 showing the colorization of the segments with smooth transitioning color schemes, and columns 3 and 4 showing the colorization of the segments with different contrasting color schemes.

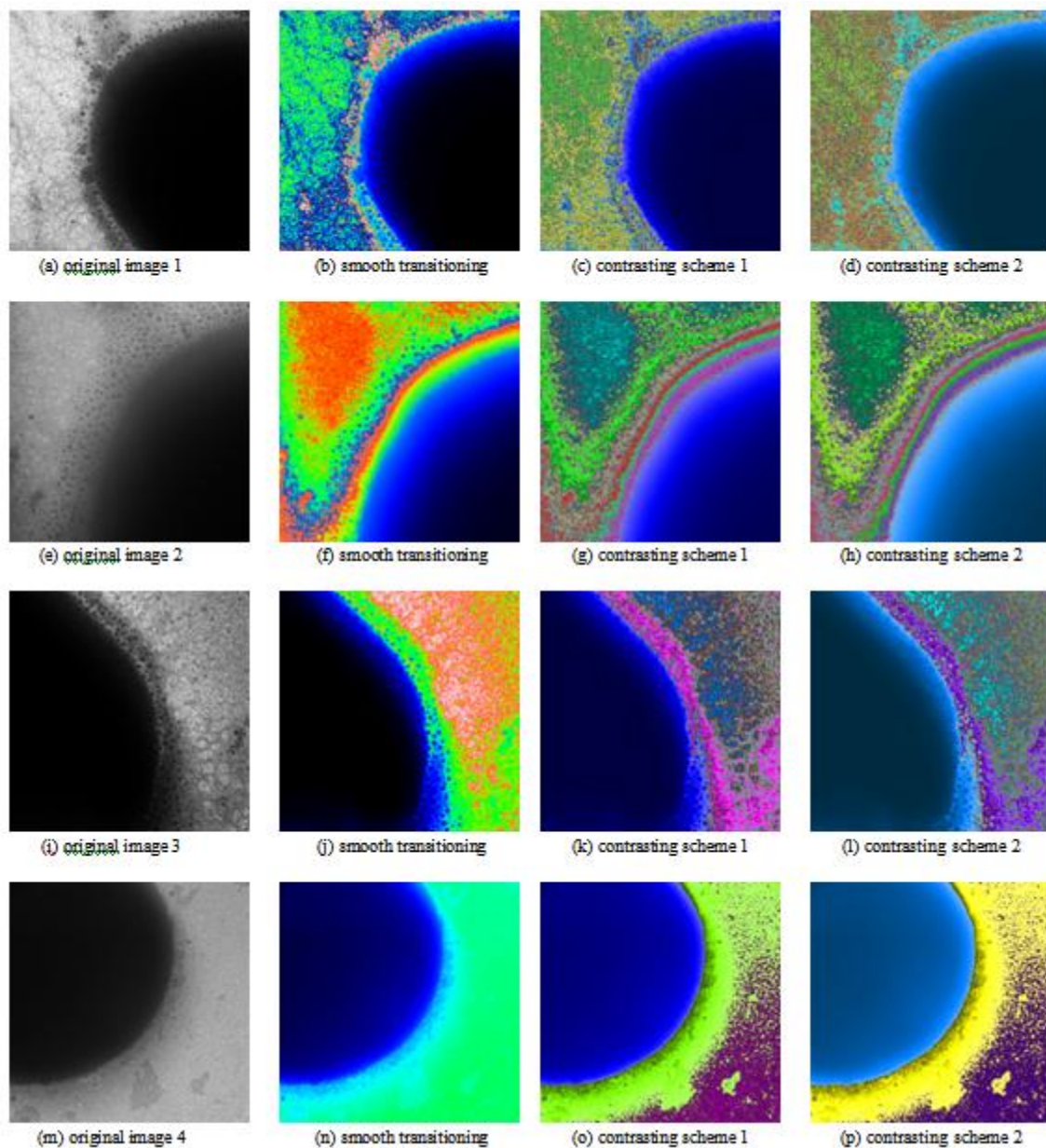


Figure 12. Segmentation of Set 2 of four electron microscope images of cells, with column 1 showing the original images, column 2 showing the colourization of the segments with smooth transitioning colour schemes, and columns 3 and 4 showing the colourization of the segments with different contrasting colour schemes.

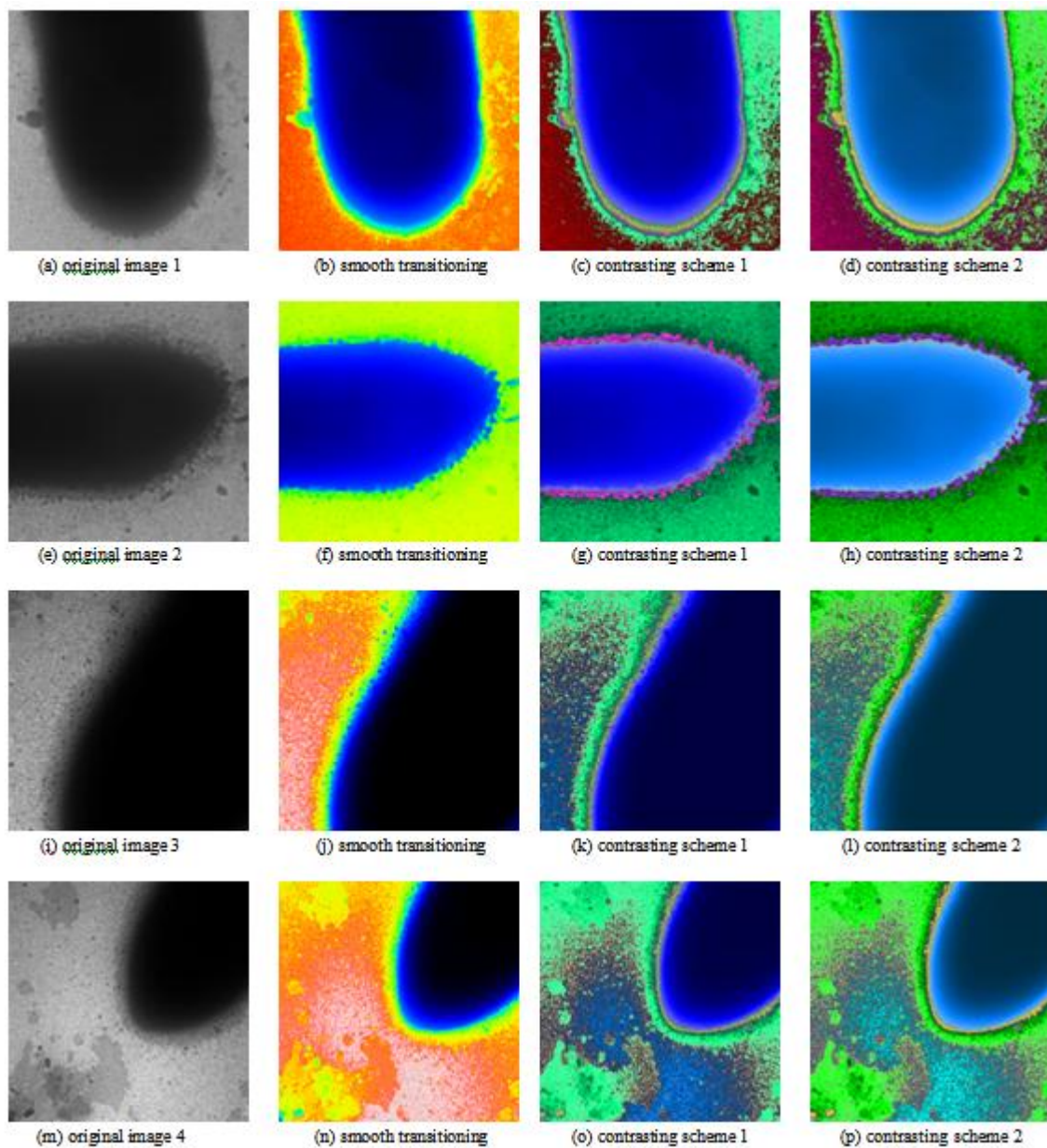


Figure 13. Segmentation of Set 3 of four electron microscope images of cells, with column 1 showing the original images, column 2 showing the colourization of the segments with smooth transitioning colour schemes, and columns 3 and 4 showing the colourization of the segments with different contrasting colour schemes.

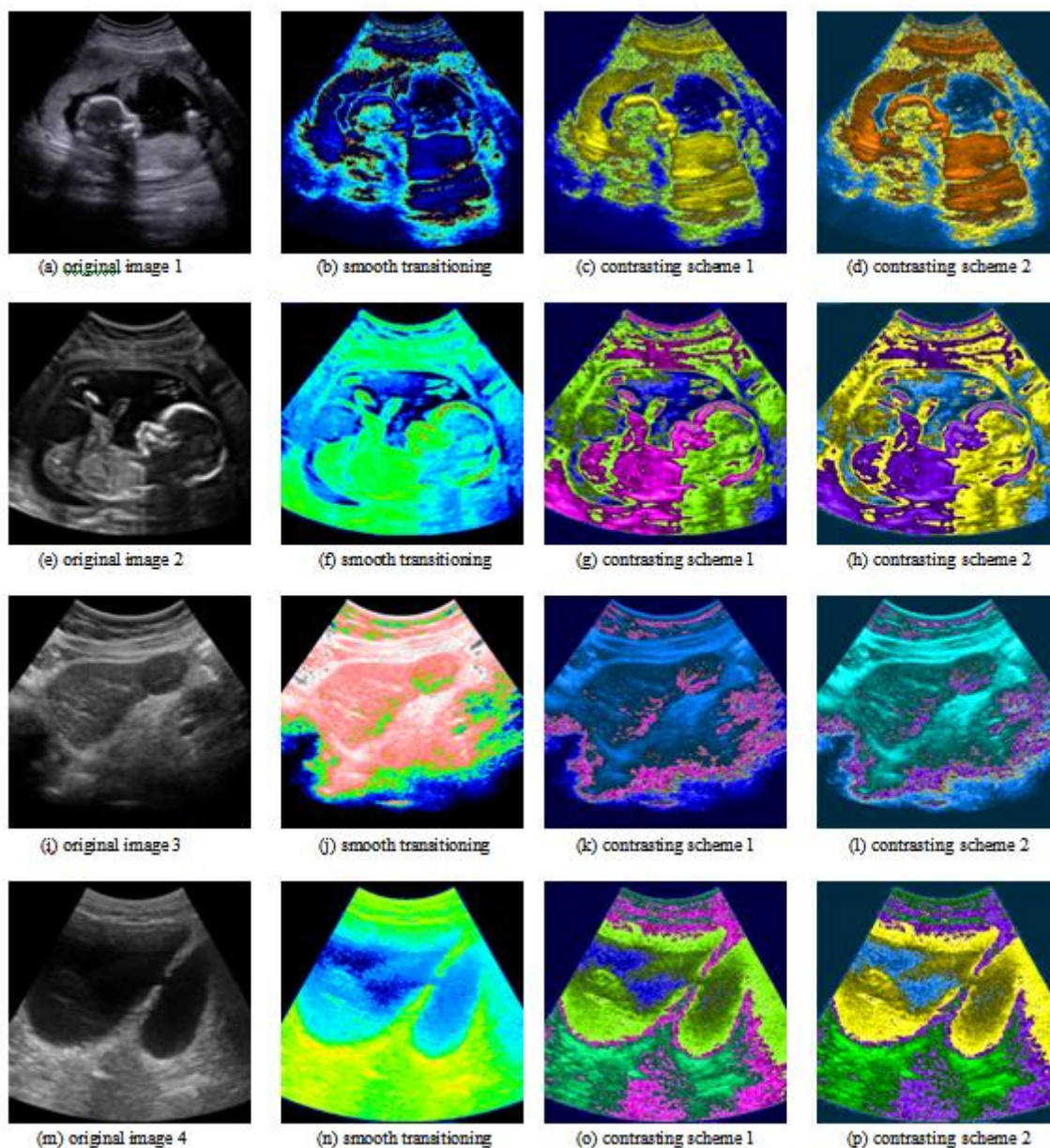


Figure 14. Segmentation of three cases of ultrasonic images: the first two rows showing the uterus of pregnant women, the third row showing a liver, and the last row showing the bladder, with column 1 showing the original images, column 2 showing the colorization of the segments with smooth transitioning colour schemes, and columns 3 and 4 showing the colorization of the segments with different contrasting color schemes.

VII. Future work: applications in thermal imaging, ultrasonic imaging, and x-ray imaging

In addition to electron microscopy, monochromatic images are commonly used for thermal imaging, ultrasonic imaging, and x-ray imaging. In this section, a few examples are presented as a demonstration of applicability of the technique to other areas that utilizes monochromatic images.

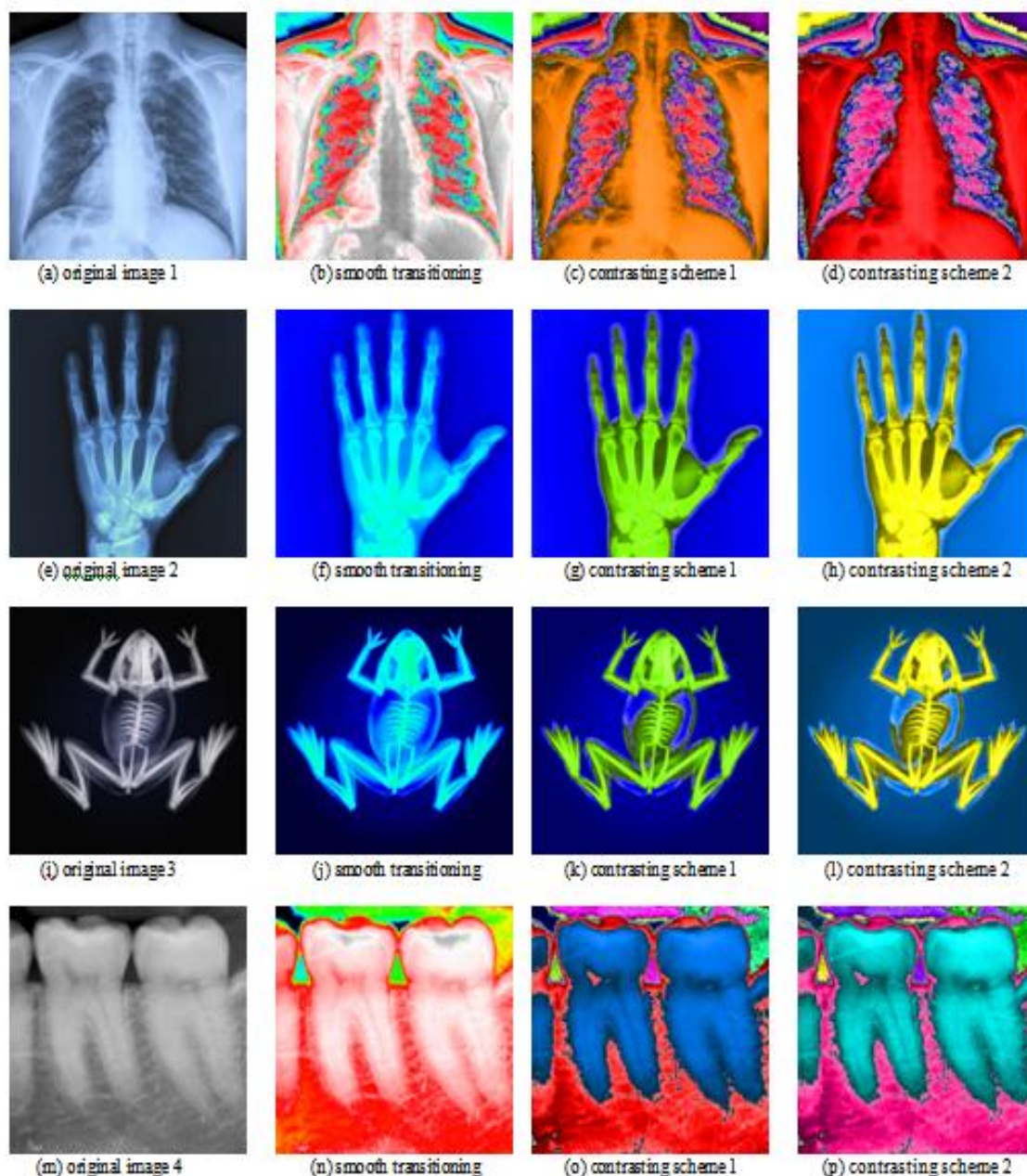


Figure 15. Segmentation of two sets of x-ray images: the first row showing the chest and lungs, the second row showing the skeleton of a frog, the third row showing human teeth, with column 1 showing the original images, column 2 showing the colourization of the segments with smooth transitioning colour schemes, and columns 3 and 4 showing the colourization of the segments with different contrasting colour schemes.

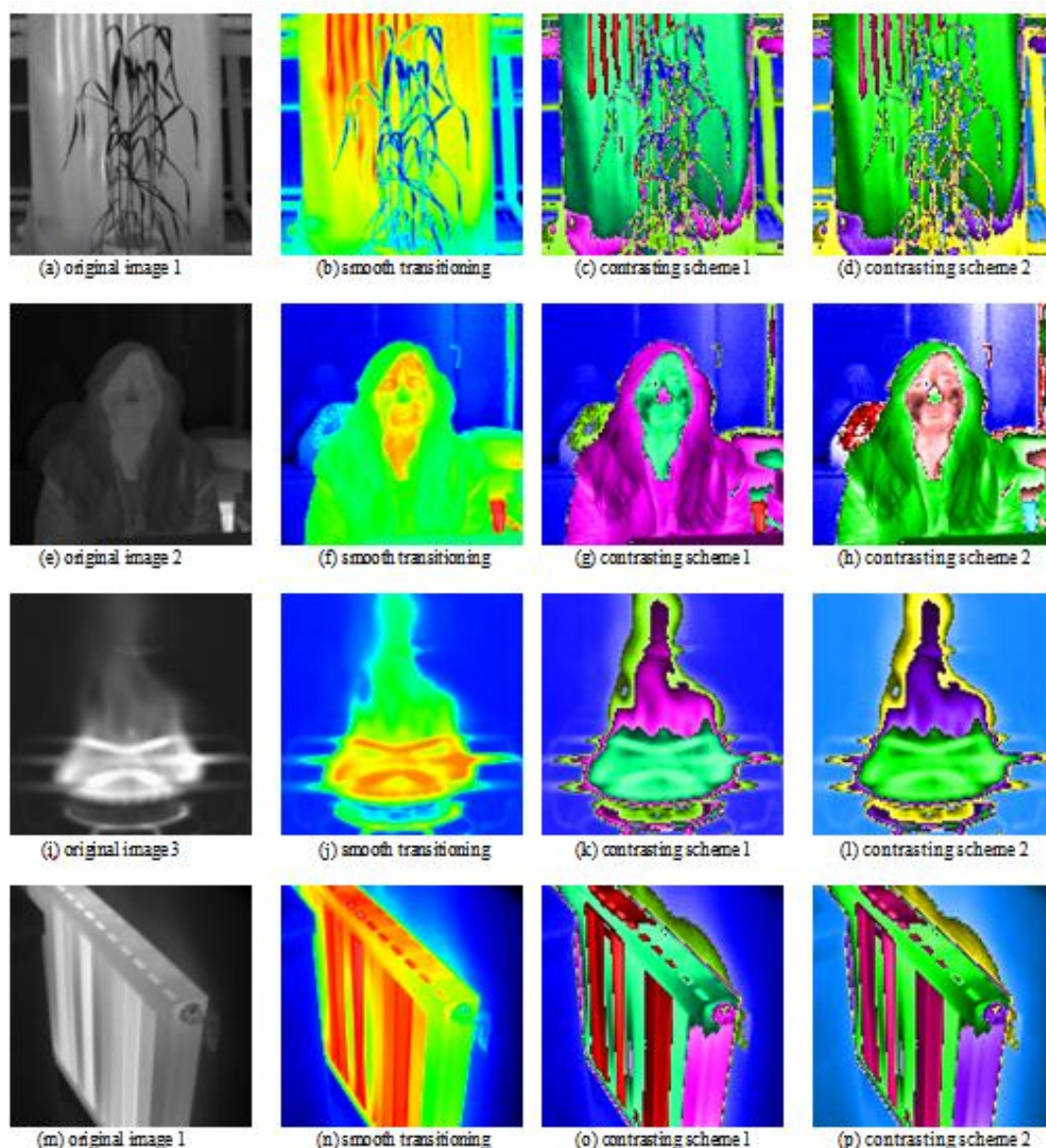


Figure 16. Segmentation of thermal images: the first row showing a plant in an agricultural study, the second row showing a person in a study of finding human in a search and rescue mission, the third row showing a burning stove in a study of detection of fire, and the fourth row showing an oil heater in an inspection routine; with column 1 showing the original images, column 2 showing the colourization of the segments with smooth transitioning colour schemes, and columns 3 and 4 showing the colourization of the segments with different contrasting colour schemes.

Ultrasonic imaging is the technique of using sounds at high frequency to scan the internal structure of a human body. The ultrasonic signal is an energy burst at the frequency just above highest frequency in the spectrum of audible sounds (above 20 kHz). The ultrasonic signal will echo (reflect back) when it encounters a disruptive boundary in the media that it is traveling through. Using this understanding, measuring the echo of the ultrasonic signal, it is possible to reconstruct the boundary of the internal structure that the ultrasonic signal is traveling through and echoing back. By looking at this boundary structure a person can get some insights of that structure. Due to the dispersion of the ultrasonic signal, the echoing often appears noisy, and for this reason the resulting images require experts to analyses. Ultrasonic imaging is common in medical application such as monitoring the growth of a baby in its mother's uterus, detecting problems of internal organs that show unusual size or shapes, etc. In Figure 14, four ultrasonic images are segmented and colorized similar to the manner that the electron microscopic images were segmented and colorized. Figures 14(a) and (e) show the original monochromatic ultrasonic images of human embryos in the uterus of pregnant women. This ultrasonic scanning procedure is common during the prenatal care. The segmentation of these images is performed, and each segment is colourized in the Figures 14(b-c) and (f-h). It is noted that the original images are noisy, and appear

like a side view of a plane cutting through the internal structure of the abdominal section of the women under the scan. While the same segments are used for all three colouring schemes, it appears that the smooth transitioning colouring scheme makes the images easier to recognize as a whole, but the contrasting colouring schemes are more helpful after the first stage of recognition of the overall image, where specific areas or parts are analysed. In this second stage, the contrasting between segments seems to improve the analysis. Figure 14(i) shows an ultrasonic image of a liver, and Figure 14(m) shows an ultrasonic image of a bladder.

X-ray imaging is the technique of using electromagnetic radiation to scan the internal structure of a human body. The x-ray signal is a burst of energy at high frequency (between 3×10^{16} Hz and 3×10^{19} Hz). The special property of signal at these frequencies is the ability to penetrate the structure, and the ability to lose some energy through the process of absorption by the media it is traveling through. The strength of the signal is measured after it is passing through and exiting a structure. By looking at x-ray images, a person can see the internal structure as if it is translucent in various degrees. X-ray imaging is commonly used to examine the bones and some internal organs not blocked by the skeletal structure. Figure 15 shows examples of x-ray images of the human lungs, human hand, frog's skeletal structure, and human teeth. Colourizing individual segments of x-ray images can certainly improve the visibility of that segment. Similar to the ultrasonic images, the x-ray images seem to give better understanding of the overall image when being coloured with smooth transitioning colours, and give better differentiating of one structure to another structure when being coloured with contrasting colours.

Thermal imaging is the technique of using infrared light (frequency between 3×10^{11} Hz and 4.3×10^{14} Hz) to scan the surface of a structure. The infrared energy is emitted by objects possessing heat, and therefore the measurement of infrared energy can be converted into temperature of the objects that emit it. By looking at an infrared image, a person can interpret the surface temperature of the objects shown in the image. Infrared imaging is commonly used in engineering applications such as inspection of equipment (heaters, water pipes, electrical wiring, computer servers, etc.), in agricultural applications such as monitoring stress in crops, in safety applications such as detection of fire, etc. The infrared energy is measured the same manner visible light is measured when it is reflected from the area of scanning, forming a two dimensional array containing infrared data. Normally, the direct measurement is converted into temperature data through some formula, and this temperature data is displayed in the form of a monochromatic image through the scaling process converting it to integers with values between 0 and 255. Manufacturers of infrared equipment often provide a simple colourization scheme assigning blue as cold temperature and red as hot temperature. In between blue and red, they use a smooth transitioning around the colour wheel in Figure 5(b) to go sequentially from blue to the colours green, yellow, orange, and red. Some manufacturers add in the colour black to indicate extremely cold, and white to indicate extremely hot. The users are trained to adapt the common sense thinking that blue is cold and red is hot to visually interpret the colourized display of thermal images. In numerical analysis, the raw data of the temperature is used. Figure 16(a) shows the monochromatic representation of a plant in a study of the effect of temperature stress, Figures 16(e) shows a face of a person in a study of recognition of human heat signature for search and rescue mission, Figure 16(i) shows a flame by a cooking stove in a study of automatic detection of fire, and Figure 16(m) shows an oil heater in a study of automatic equipment inspection. The corresponding images in the same row as the monochromatic representation are the colourization in various colouring schemes. The smooth transitioning scheme again seems to give a better depiction of the reality helping an analyst to correlate to the object as if seen directly by human eyes. The contrasting scheme seems to help an analyst to study individual parts of an object for detailed analysis afterward.

VIII. Conclusion

It has been shown that segmentation of an image can be done automatically on the non-iterative basis without a priori knowledge of the number of segments at the beginning of the process. These characteristics are achieved through the method of artificial gravitational field in the histogram space of colors where each pixel is assigned an arbitrary mass that can exert pulling gravitational effect on other pixels in that space. The calculated field values are used to determine if two adjacent pixel values are converging toward a common convergent point and thus are assigned to the same group, or diverging away from each other and thus are assigned to different groups. When segments are identified, they can be colorized in the manner to enhance their visibility to allow human to analyses the images with efficiency. Examples are given in electron microscopic images to demonstrate the workability of the concept, and additional examples in x-ray imaging, ultrasonic imaging, and thermal imaging are given to demonstrate the applicability of the concept to other areas that utilize monochromatic images.

References

- [1]. Stirling, J., Curry, A., and Eyden, B. (2013). *Diagnostic electron microscopy: a practical guide to interpretation and technique*. West Sussex, UK: John Wiley & Sons. ISBN-13: 978-1119973997.
- [2]. Viswanathan, P. (2011). *Electron microscopy*. Chennai, India: MJP Publishers. ISBN-13: 978-8180940750.
- [3]. Bozzola, J. J., and Russell, L. D. (1998). *Electron microscopy*. Toronto, ON (Canada): Jones & Bartlett Publishers. ISBN-13: 978-0763701925.
- [4]. Hunter, E. E. (1993). *Practical electron microscopy: a beginner's illustrated guide*. Cambridge, UK: Cambridge University Press. ISBN-13: 978-0521385398.
- [5]. Egerton, R. F. (2016). *Physical principles of electron microscopy: an introduction to TEM, SEM, and AEM*. New York, NY: Springer. ISBN-13: 978-3319398761.
- [6]. Egerton, R. F. (2011). *Electron energy-loss spectroscopy in the electron microscope*. New York, NY: Springer. ISBN-13: 978-1441995827.
- [7]. Khursheed, A. (2010). *Scanning electron microscope optics and spectrometer*. Singapore: World Scientific Publishing Company. ISBN-13: 978-9812836670.
- [8]. Champness, P. E. (2001). *Electron diffraction in the transmission electron microscope*. New York, NY: Taylor & Francis. ISBN-13: 978-1859961476.
- [9]. Mandal, A. K. (2014). *Electron microscopy of the kidney: in renal disease and hypertension: a clinicopathological approach*. New York, NY: Springer. ISBN-13: 978-1475717013.
- [10]. Schatten, H. (2013). *Scanning electron microscopy for the life sciences*. New York, NY: Cambridge University Press. ISBN-13: 978-0521195997.
- [11]. Motta, P. (2013). *Ultrastructure of endocrine cells and tissues (electron microscopy in biology and medicine)*. New York, NY: Springer. ISBN-13: 978-1461338635.
- [12]. Dykstra, M. J., and Reuss, L. E. (2003). *Biological electron microscopy: theory, techniques, and troubleshooting*. New York, NY: Springer. ISBN-13: 978-0306477492.
- [13]. Bozzola, J. J., and Russell, L. D. (1992). *Electron microscopy: principles and techniques for biologists*. Toronto, ON (Canada): Jones & Bartlett Publishers. ASIN: B008W5X83Q.
- [14]. Sabnis, R. W. (2015). *Handbook of fluorescent dyes and probes*. Hoboken, NJ: John Wiley & Sons. ISBN-13: 978-1118028698.
- [15]. Waters, J., and Wittmann, T. (2014). *Quantitative imaging in cell biology*. Waltham, MA: Academic Press. ISBN-13: 978-0124201385.
- [16]. Sabnis, R. W. (2010). *Handbook of biological dyes and stains: synthesis and industrial applications*. Hoboken, NJ: John Wiley & Sons. ISBN-13: 978-0470407530.
- [17]. Horobin, R., and Kiernan, J. (2002). *Conn's biological stains: a handbook of dyes, stains and fluorochromes for use in biology and medicine*. Oxford, UK: BIOS Scientific Publishers. ISBN-13: 978-1859960998.
- [18]. Liu, S. M., Chen, C. F., and Chou, K. C. (May 2011). "The design and implementation of a low-cost 360-degree color LED display system." *IEEE transactions on consumer electronics*, vol. 57, no. 2, pp. 289-296. doi: 10.1109/TCE.2011.5955158.
- [19]. Borodkin, S. M., Borodkin, A. M., and Muchnik, I. B. (Feb. 2006). "Optimal requantization of deep grayscale images and Lloyd-Max quantization." in *IEEE transactions on image processing*, vol. 15, no. 2, pp 445-448. doi: 10.1109/TIP.2005.860611.
- [20]. Vander Kam, R. A., Wong, P. W., and Gray, R. M. (Jan. 1999). "JPEG-compliant perceptual coding for a grayscale image printing pipeline." *IEEE transactions on image processing*, vol. 8, no. 1, pp. 1-14. doi: 10.1109/83.736675.
- [21]. Yu, S. S., and Galatsanos, N. P. (Feb 1996). "Binary decompositions for high-order entropy coding of grayscale images." *IEEE transactions on circuits and systems for video technology*, vol. 6, no. 1, pp 21-31. doi: 10.1109/76.486417.
- [22]. Liu, S. M., Chen, C. F., and Chou, K. C. (May 2011). "The design and implementation of a low-cost 360-degree color LED display system." *IEEE transactions on consumer electronics*, vol. 57, no. 2, pp. 289-296. doi: 10.1109/TCE.2011.5955158.
- [23]. Nazeran Motlagh, A., Hashemi, M. R., and Hoseinifar, M. (Nov. 2011). "A novel design for 3-color LED display panel based on CPU processor." *IEEE journal of display technology*, vol. 7, no. 11, pp. 607-614. doi: 10.1109/JDT.2011.2159191.
- [24]. Yost, B., Haciahmetoglu, Y., and North, C. (2007). "Beyond visual acuity: the perceptual scalability of information visualizations for large displays." *Proceedings of the SIGCHI conference on human factors in computing systems*, pp 101-110. doi: 10.1145/1240624.1240639.
- [25]. Westheimer, G. (1972). "Visual acuity and spatial modulation thresholds." *Handbook of sensory physiology*, vol. 7, no. 4, pp 170-187. doi: 10.1007/978-3-642-88658-4_7.
- [26]. Cavonius, C. R., and Schumacher, A. W. (May 1966). "Human visual acuity measured with colored test objects." *AAAS journal science*, vol. 152, no. 3726, pp 1276-1277. doi:10.1126/science.152.3726.1276.
- [27]. Campbell, F. W., and Kulikowski, J. J. (Nov. 1966). "Orientational selectivity of the human visual system." *The journal of physiology*, vol. 187, no. 2, pp 437-445. PMID: PMC1395934.
- [28]. Wu, H. C., Chiu, M. C., Jian, J. H. (Jun. 2016). "Evaluation of four eyestrain recovery methods for visual display terminal workers." *Communications in computer and information science*, vol. 617, pp 536-541. doi:10.1007/978-3-319-40548-3_89.
- [29]. Thorud, H. M. S., Helland, M., Aarås, A., Kvikstad, T. M., Lindberg, L. G., and Horgen, G. (Apr. 2012). "Eye-related pain induced by visually demanding computer work." *Optometry & vision science*, vol. 89, no. 4, pp 452-464. doi: 10.1097/OPX.0b013e31824c1801.
- [30]. Björklund, M., Crenshaw, A. G., Djupsjöbacka, M., and Johansson, M. (Feb. 2000). "Position sense acuity is diminished following repetitive low-intensity work to fatigue in a simulated occupational setting." *European journal of applied physiology*, vol. 81, no. 5, pp 361-367. doi: 10.1007/s004210050055.
- [31]. Christensen, H., Sogaard, K., Pilegaard, M. and Olsen, H. B. (May 2000). "The importance of the work/rest pattern as a risk factor in repetitive monotonous work." *International journal of industrial ergonomics*, vol. 25, no. 4, pp 367-373. doi:10.1016/S0169-8141(99)00025-6.
- [32]. Hodgson, A., Siemieniuch, C. E., and Hubbard, E. M. (Nov. 2013). "Culture and the safety of complex automated sociotechnical systems." *IEEE transactions on human-machine systems*, vol. 43, no. 6, pp 608-619. doi: 10.1109/THMS.2013.2285048.
- [33]. Piloti, M., and Chodorow, M. (May 2012). "Does familiarity with text breed complacency or vigilance?" *Journal of research in reading*, vol. 35, no. 2, pp 204-214. doi: 10.1111/j.1467-9817.2010.01462.x.
- [34]. Jacinto, C., Canoa, M., Guedes Soares, C. (May 2009). "Workplace and organisational factors in accident analysis within the Food Industry." *Safety science*, vol. 47, no. 5, pp 626-635. doi:10.1016/j.ssci.2008.08.002.
- [35]. Singh, I. L., Molloy, R., and Parasuraman, R. (Nov. 2009). "Automation-induced 'complacency': development of the complacency-potential rating scale." *The international journal of aviation psychology*, vol. 3, no. 2, pp 111-122. doi: 10.1207/s15327108ijap0302_2.

- [36]. Yue, C. L., Storm, B. C., Kornell, N., and Bjork, E. L. (Mar. 2015). "Highlighting and its relation to distributed study and students' metacognitive beliefs." *Educational psychology review*, vol. 27, no. 1, pp 69-78. doi 10.1007/s10648-014-9277-z.
- [37]. Robinson, A. C. (Mar. 2013). "Highlighting in geovisualization." *Cartography and geographic information science*, vol. 38, no. 4, pp 373-383. doi: 10.1559/15230406384373.
- [38]. Dunlosky, J., awson, K. A., Marsh, E. J., Nathan, M. J., and Willingham, D. T. (2013). "Improving students' learning with effective learning techniques: promising directions from cognitive and educational psychology." *Psychological science in the public interest*, vol. 14, no. 1, pp. 4-58. doi: 10.1177/1529100612453266.
- [39]. Nist, S. L., and Kirby, K. (1989). "The text marking patterns of college students." *Reading psychology: an international quarterly*, vol. 10, no. 4, pp. 321-338. doi:10.1080/0270271890100403.
- [40]. Wu, J. H., and Yuan, Y. (August 2003). "Improving searching and reading performance: the effect of highlighting and text color coding." *Information and management*, vol. 40, no. 7, pp 617-637. doi: 10.1016/S0378-7206(02)00091-5.
- [41]. Schilit, B. N., Golovchinski, G., and Price, M. N. (April 1998). "Beyond paper: supporting active reading with free form digital ink annotations." *Proceedings of the SIGCHI conference on human factors in computing systems*, pp 249-256. doi: 10.1145/274644.274680.
- [42]. Mayer, R. E., Steinhoff, K., Bower, G., and Mars, R. (March 1995). "A generative theory of textbook design: Using annotated illustrations to foster meaningful learning of science text." *Educational technology research and development*, vol. 43, no. 1, pp 31-41. doi: 10.1007/BF02300480.
- [43]. Pastoor, S. (1990). "Legibility and subjective preference for color combinations in text." *Human factors*, vol. 32, no. 2, pp 157-171. doi: 10.1177/001872089003200204.
- [44]. Thorne, K. S., & Blandford, R. D. (2017). *Modern Classical Physics: Optics, Fluids, Plasmas, Elasticity, Relativity, and Statistical Physics*. Princeton, NJ: Princeton University Press. ISBN-10 : 0691159025.
- [45]. Shankar, R. (2014). *Fundamentals of Physics: Mechanics, Relativity, and Thermodynamics*. New Haven, CT: Yale University Press.

Jonathan Tri Pham. "Segmentation of Electron Microscopic Images with Artificial Gravitational Field for Enhancement of Visibility." *IOSR Journal of Computer Engineering (IOSR-JCE)*, 22(5), 2020, pp. 12-31.